HVDC Grid Protection Algorithm Design in Phase and Modal Domains

W. Leterme, S. Pirooz Azad, D. Van Hertem

DOI: 10.1049/iet-rpg.2018.5163

IET Journals
The Institution of Engineering and Technology

HVDC Grid Protection Algorithm Design in Phase and Modal Domains

ISSN 1751-8644
doi: 0000000000
www.ietdl.org

W. Leterme[1,2] *S. Pirooz Azad*[3] *D. Van Hertem*[1,2]

[1] *Dept. of Electrical Engineering, KU Leuven, Kasteelpark Arenberg 10 (PB2445), 3000 Leuven, Belgium*
[2] *EnergyVille, Thor Park 8310, 3600 Genk, Belgium*
[3] *Electrical and Computer Engineering, University of Waterloo, Waterloo, ON, Canada*
** E-mail: willem.leterme@esat.kuleuven.be*

Abstract: To meet the required operation speed for protection of meshed voltage source converter (VSC) high voltage direct current (HVDC) grids, traveling wave-based algorithms operating in the sub-millisecond time-frame can be used. The domain in which these algorithms operate, i.e., modal or phase, determines their performance in fault discrimination, fault type classification and faulted pole selection. In the recent literature, high-speed algorithms have been proposed for various VSC HVDC grid configurations and transmission line types; yet the choice of domain has received insufficient attention. This paper offers recommendations for the choice of domain for protection algorithm design of HVDC overhead line or cable systems in symmetric monopolar and bipolar configurations. The theoretical analysis of this paper, which is based on fundamental wave propagation theory, indicates that the preferred domain for protection algorithms for cable and overhead line systems are the phase and modal, respectively. Furthermore, the paper provides comprehensive guidelines to construct detection functions for both configurations and discusses the errors introduced by approximations. Finally, study results from a bipolar overhead line test system demonstrate the advantages of modal over phase domain for fast fault discrimination and classification and illustrate practical problems associated with non-ideal detection functions.

1 Introduction

The high-voltage direct current (HVDC) grid has attracted considerable attention in Europe and China. At present, the closest infrastructure to an HVDC grid is the five-terminal link in Zhoushan, China, which was commissioned in 2014. However, an HVDC grid is yet to be realized in practice. Protection is one of the technical challenges that should be addressed to facilitate the realization of HVDC grids. For large-scale meshed HVDC grids, protection can be obtained by utilizing selective algorithms as well as HVDC breakers at two ends of all transmission lines.

The speed of the protection algorithm plays a critical role in the design of selective HVDC grid protection [1]. Fast protection enables the use of slower HVDC breakers as well as decreasing the size of fault current limiting equipment. Furthermore, fast protection inhibits a large decrease of the dc voltage in the healthy part of the grid [2].

In the design of protection algorithms, the choice of modal or phase domain determines the ability of the algorithm to timely detect faults and identify their type. Ideally, the algorithms discriminate between faults on the line to be protected and external ones, identify the correct fault type and select the faulted pole(s). As such, only the breakers on the faulted pole(s) are tripped.

In the recent literature on protection algorithms for HVDC grids, e.g., in [3–14], various grid configurations are studied but the selection of the appropriate domain for protection algorithm design has received insufficient attention. For protection algorithms applied to VSC HVDC grids, the wave propagation characteristics in each domain depend on the combination of HVDC grid configuration, i.e., asymmetric monopole, symmetric monopole or bipole, and transmission line type, i.e., cable and overhead line. Protection algorithm design for HVDC grids has been mainly based on extensive time-domain simulations with detailed models for a specific configuration. Although this is an essential step in threshold setting and final engineering of a protection algorithm, a general approach towards the selection of the optimal domain for HVDC grid protection considering various grid and transmission line configurations is still missing.

This paper offers recommendations for the selection of the domain to design selective protection algorithms for HVDC grids with overhead line and cable systems as well as symmetric monopole and bipolar configurations. These recommendations are based on traveling wave theory and analysis of wave propagation characteristics. Furthermore, this paper provides comprehensive guidelines to form detection functions in the appropriate domain. These guidelines are verified through simulation studies and considerations for practical application in an HVDC grid are provided.

2 Review of Existing Protection Algorithms

Various algorithms have been proposed for the protection of dc power systems with line-commutated converters (LCCs) and voltage source converters (VSCs). For each type of dc system, this section gives a brief overview of the proposed algorithms and discusses the advantages and disadvantages of each domain for protection algorithm design.

2.1 LCC dc-systems

In LCC-dc systems, most of the proposed algorithms are designed for systems with overhead transmission lines in a bipolar configuration without metallic return. These algorithms can be categorized into phase domain and modal domain approaches.

2.1.1 Phase Domain: Several algorithms which use quantities in the phase domain are reported for the protection of LCC-dc systems [15–20]. The algorithms reported in [15–18] are similar in nature, where the dc voltage and its derivative are compared against thresholds and possibly complemented by a threshold on the current derivative. Although in [15, 17], the use of the phase domain is not explicitly mentioned, statements and schemes found in [16, 21, 22] imply that these functions are implemented on a per pole basis. The detection time and the thresholds are chosen to discriminate line faults from converter and ac faults as well as to prevent the trip of the healthy pole. In [16], a detection time of 3 ms is reported.

The algorithms proposed in [19] and [20] use voltage measurements to distinguish between faulted and healthy poles by assessing whether the pole voltage has a transient nature (healthy pole) or not (faulted pole). The time windows to make a decision on the faulted pole is 3 ms in [19] and 10 ms in [20].

2.1.2 Modal Domain: The algorithms developed in the modal domain, [23–28], mainly use the aerial or metallic mode for fault detection and discrimination, whereas the polarity of the ground mode is used to identify the faulted pole [29]. An exception to this approach is discussed in [23], where modal quantities are used to mitigate the mutual coupling between poles and selection of the faulted pole is based on the pole voltages in the phase domain. The algorithms are either non-unit protection [23–26] or differential [27]. The reported detection times are 1 ms in [25] and 5 ms in [23, 26].

2.2 VSC dc-systems

A comprehensive overview of protection algorithms developed for dc grids, which are based on VSCs, is given in [30]. These algorithms are developed for systems with cable and overhead transmission lines.

Phase Domain: Several algorithms for VSC-dc systems with cables are reported in the literature [3–14]. However, the choice of domain for the algorithm development is only specified for [13]. The algorithms proposed in [3–8], which use current derivatives or filters implementing a similar function, are non-unit protection. The algorithms proposed in [9–12] are current differential, whereas the one proposed in [13] is a traveling wave differential algorithm. The algorithm proposed in [14] uses the polarity of the current wave for fault detection. In [7], the same algorithm proposed for cable systems is applied to overhead lines, without any modifications to the threshold settings as well as fault type classification and faulted pole selection criteria.

Modal Domain: The application of voltage and current derivatives in the modal domain for fault detection of cable systems is investigated in [31]. The choice of modal domain is motivated by the balanced cable configuration in the studied symmetrical monopolar test system. To the best of our knowledge, no algorithms based on modal quantities are proposed for protection of overhead line systems.

2.3 Discussion

The review of existing literature shows that for LCC- and VSC-dc transmission systems with cables or overhead lines, protection algorithms in both phase and modal domains have been proposed.

In LCC-dc overhead line systems with two conductors, the reason for selecting the modal domain is to decouple the ground mode from the aerial mode and to use the polarity of the former one to determine the faulted pole. The algorithms developed in both domains typically use a time window exceeding 3 ms, with the exception of [25]. Time windows exceeding a few milliseconds are long in comparison with HVDC circuit breaker opening times of 2-5 ms.

For VSC-dc systems, algorithms for both overhead line and cables are proposed in the phase domain, whereas the modal domain is only used for cable systems in [13]. In [13], the modal domain is only recommended for balanced line configurations whereas no discussion is provided on the particularities associated with cable or overhead line systems.

The remainder of the paper focuses on providing recommendations for the selection of the domain in the design of fast protection algorithms for HVDC grids. The recommendations take into account HVDC grid configuration and the transmission line type.

3 Fault Analysis in Phase and Modal Domains

This section provides the background theory with respect to fault analysis, wave propagation and construction of fault detection functions for traveling wave-based protection algorithms.

3.1 Fault Wave Inception and Propagation

3.1.1 First Incident Wave Voltage at the Fault Location for Solid Faults: In the phase domain, the relationship between the voltage and current of the first wave traveling from the fault location, $\boldsymbol{U}_{\mathrm{f}}$ and $\boldsymbol{I}_{\mathrm{f}}$, can be described as:

$$\boldsymbol{U}_{\mathrm{f}} = \boldsymbol{Z}_{\mathrm{c,phase}} \boldsymbol{I}_{\mathrm{f}}, \tag{1}$$

where $\boldsymbol{Z}_{\mathrm{c,phase}}$ is the characteristic impedance in the phase-domain. For a solid pole-to-ground fault at pole k,

$$\begin{aligned} U_{\mathrm{f}}^{(k)} &= -U_{\mathrm{pre}}^{(k)}, \\ I_{\mathrm{f}}^{(k)} &= -\frac{I_{\mathrm{flt}}}{2}, \\ I_{\mathrm{f}}^{(l)} &= 0, \ \forall\, l \neq k, \end{aligned} \tag{2}$$

where $U_{\mathrm{pre}}^{(k)}$ is the pre-fault voltage at pole k and I_{flt} is the current flowing into the fault (before any reflected fault wave has reached the fault location). Substituting (2) into (1) gives the voltage at the fault location at pole t:

$$U_{\mathrm{f}}^{(t)} = -\frac{Z_{\mathrm{c}}^{(t,k)}}{Z_{\mathrm{c}}^{(k,k)}} U_{\mathrm{pre}}^{(k)}, \tag{3}$$

where the superscripts (t,k) and (k,k) are associated with the corresponding elements in $\boldsymbol{Z}_{\mathrm{c,phase}}$. In the phase domain, for a pole-to-ground fault, the voltage of the first incident traveling wave at each pole can be calculated using (3).

For a solid pole-to-pole fault between poles k and l, the following conditions apply:

$$\begin{aligned} U_{\mathrm{f}}^{(k)} - U_{\mathrm{f}}^{(l)} &= -(U_{\mathrm{pre}}^{(k)} - U_{\mathrm{pre}}^{(l)}), \\ I_{\mathrm{f}}^{(k)} &= -\frac{I_{\mathrm{flt}}}{2}, \\ I_{\mathrm{f}}^{(l)} &= \frac{I_{\mathrm{flt}}}{2}, \\ I_{\mathrm{f}}^{(m)} &= 0, \ \forall\, m \neq k, l. \end{aligned} \tag{4}$$

Substituting (4) in (1) and defining $U_{\mathrm{pre}}^{(k,l)} = U_{\mathrm{pre}}^{(k)} - U_{\mathrm{pre}}^{(l)}$, gives for pole t:

$$U_{\mathrm{f}}^{(t)} = -\frac{Z_{\mathrm{c}}^{(t,k)} - Z_{\mathrm{c}}^{(t,l)}}{Z_{\mathrm{c}}^{(k,k)} + Z_{\mathrm{c}}^{(l,l)} - 2Z_{\mathrm{c}}^{(k,l)}} U_{\mathrm{pre}}^{(k,l)}. \tag{5}$$

3.1.2 Wave Propagation: In general, HVDC cables and overhead lines are multi-conductor transmission line systems, of which the theory is extensively described in [32], but briefly recapitulated here. In a multi-conductor transmission line system, voltages and currents can be described using the wave equations:

$$\begin{aligned} \frac{d^2}{dz^2} \boldsymbol{U}_{\mathrm{phase}}(z) &= \boldsymbol{Z}_{\mathrm{phase}} \boldsymbol{Y}_{\mathrm{phase}} \boldsymbol{U}_{\mathrm{phase}}(z) \\ \frac{d^2}{dz^2} \boldsymbol{I}_{\mathrm{phase}}(z) &= \boldsymbol{Y}_{\mathrm{phase}} \boldsymbol{Z}_{\mathrm{phase}} \boldsymbol{I}_{\mathrm{phase}}(z), \end{aligned} \tag{6}$$

where $\boldsymbol{U}_{\mathrm{phase}}(z)$ and $\boldsymbol{I}_{\mathrm{phase}}(z)$ are voltage and current vectors at location z of the line in the phase domain and $\boldsymbol{Y}_{\mathrm{phase}}$ and $\boldsymbol{Z}_{\mathrm{phase}}$ are per unit length shunt admittance and series impedance matrices,

respectively. The wave propagation constant matrix of the transmission line is given by $\boldsymbol{\Gamma} = \sqrt{\boldsymbol{Y}_{\text{phase}}\boldsymbol{Z}_{\text{phase}}}$. Using eigenvalue theory, $\boldsymbol{\Gamma}^2$ can be represented as $\boldsymbol{T}_{\text{i}}\boldsymbol{\Lambda}\boldsymbol{T}_{\text{i}}^{-1}$, where $\boldsymbol{T}_{\text{i}}$ is the matrix of eigenvectors of $\boldsymbol{\Gamma}^2$ and $\boldsymbol{\Lambda}$ is a diagonal matrix with the eigenvalues of $\boldsymbol{\Gamma}^2$ on the diagonal.

The coupled equations of the multi-conductor system with n conductors can be transformed into n decoupled single-phase equations. The transformation of the coupled equations in the phase domain to decoupled equations in the modal domain is performed through modal decomposition. The multi-conductor system can be described in the modal domain using:

$$-\frac{d^2}{dz^2}\boldsymbol{U}_{\text{mode}}(z) = \boldsymbol{\Lambda}\boldsymbol{U}_{\text{mode}}(z) \tag{7}$$

$$-\frac{d^2}{dz^2}\boldsymbol{I}_{\text{mode}}(z) = \boldsymbol{\Lambda}\boldsymbol{I}_{\text{mode}}(z), \tag{8}$$

where $\boldsymbol{U}_{\text{mode}}(z)$ and $\boldsymbol{I}_{\text{mode}}(z)$ are voltage and current vectors of length n in the modal domain. The transformation from phase domain to modal domain is obtained via:

$$\boldsymbol{U}_{\text{phase}} = \boldsymbol{T}_{\text{u}}\boldsymbol{U}_{\text{mode}} \tag{9}$$

$$\boldsymbol{I}_{\text{phase}} = \boldsymbol{T}_{\text{i}}\boldsymbol{I}_{\text{mode}}, \tag{10}$$

where, for n distinct eigenvalues, it is proven that $[\boldsymbol{T}_{\text{u}}]^{-1} = [\boldsymbol{T}_{\text{i}}]^{\text{T}}$ [33]. $\boldsymbol{T}_{\text{u}}$ and $\boldsymbol{T}_{\text{i}}$ are known as modal transformation matrices.

The characteristic impedance of the transmission line can be described in the phase or modal domain and is given by:

$$\boldsymbol{Z}_{\text{c,phase}} = \boldsymbol{Z}_{\text{phase}}\sqrt{(\boldsymbol{Y}_{\text{phase}}\boldsymbol{Z}_{\text{phase}})^{-1}} \tag{11}$$

$$\boldsymbol{Z}_{\text{c,mode}} = \sqrt{\frac{\boldsymbol{Z}_{\text{mode}}}{\boldsymbol{Y}_{\text{mode}}}}, \tag{12}$$

in which $\boldsymbol{Z}_{\text{mode}} = \boldsymbol{T}_{\text{u}}^{-1}\boldsymbol{Z}_{\text{phase}}\boldsymbol{T}_{\text{i}}$ and $\boldsymbol{Y}_{\text{mode}} = \boldsymbol{T}_{\text{i}}^{-1}\boldsymbol{Y}_{\text{phase}}\boldsymbol{T}_{\text{u}}$ and $\boldsymbol{Z}_{\text{c,mode}}$ is a diagonal matrix [34].

3.1.3 First Incident Wave Voltage at the Relay Location:

The voltage at the relay location $\boldsymbol{U}_{\text{r}}$ (receiving end) is related to the voltage $\boldsymbol{U}_{\text{f}}$ at the fault location (sending end) through:

$$\boldsymbol{U}_{\text{r}} - \boldsymbol{Z}_{\text{c,phase}}\boldsymbol{I}_{\text{r}} = (\boldsymbol{U}_{\text{f}} + \boldsymbol{Z}_{\text{c,phase}}\boldsymbol{I}_{\text{f}})e^{-\boldsymbol{\Gamma}'l}, \tag{13}$$

where l is the distance between fault and relay location and $\boldsymbol{\Gamma}' = \sqrt{\boldsymbol{Z}_{\text{phase}}\boldsymbol{Y}_{\text{phase}}}$.

3.2 Traveling Wave-Based Protection Algorithm Design

In traveling wave-based protection algorithms, detection functions can be constructed in the phase or modal domain to separate the traveling waves originating from disturbances in the forward or backward direction of the relay, respectively. In this paper, detection functions $\boldsymbol{D}_{\text{phase}}^{\text{f,b}}$ and $\boldsymbol{D}_{\text{mode}}^{\text{f,b}}$ are defined as [35, 36]:

$$\boldsymbol{D}_{\text{phase}}^{\text{f,b}} = \boldsymbol{U}_{\text{r}} \mp \boldsymbol{R}_{\text{c,phase}}\boldsymbol{I}_{\text{r}}, \tag{14}$$

$$\boldsymbol{D}_{\text{mode}}^{\text{f,b}} = \hat{\boldsymbol{T}}_{\text{u}}^{-1}\boldsymbol{U}_{\text{r}} \mp \boldsymbol{R}_{\text{c,mode}}\hat{\boldsymbol{T}}_{\text{i}}^{-1}\boldsymbol{I}_{\text{r}}, \tag{15}$$

where $\boldsymbol{D}^{\text{f}}$ and $\boldsymbol{D}^{\text{b}}$ are (considering a relay at a transmission line end and the positive value of $\boldsymbol{I}_{\text{r}}$ for currents flowing into the line) associated with waves originating from faults in the forward and backward directions of the relay, respectively. $\boldsymbol{R}_{\text{c,phase}}$ and $\boldsymbol{R}_{\text{c,mode}}$ are replica surge impedances associated with $\boldsymbol{Z}_{\text{c,phase}}$ and $\boldsymbol{Z}_{\text{c,mode}}$. $\hat{\boldsymbol{T}}_{\text{u}}$ and $\hat{\boldsymbol{T}}_{\text{i}}$ are approximations for the voltage and current transformation matrices.

In the remainder of this paper, the focus will be on forward detection functions and the first incident wave. With these detection functions, the algorithms can identify faults independent from the termination impedance.

3.3 Sources of Error

3.3.1 Error due to Approximation of Characteristic Impedance:

In case $\boldsymbol{R}_{\text{c}}$ perfectly matches $\boldsymbol{Z}_{\text{c}}$, $\boldsymbol{D}^{\text{f}}$ and $\boldsymbol{D}^{\text{f}}$ will become termination-independent and will precisely discriminate between waves in forward and backward directions. In such a case, $\boldsymbol{D}^{\text{f}}$ and $\boldsymbol{D}^{\text{f}}$ will take a value twice the incident voltage and zero for waves in their foward and backward directions, respectively (see (13) and also [37]). In general, detection functions $\boldsymbol{D}^{\text{f}}$ and $\boldsymbol{D}^{\text{f}}$ will take a small non-zero value and one lower than twice the incoming wave for waves initiated from a fault in the reverse and forward directions, since $\boldsymbol{R}_{\text{c}}$ does not necessarily match $\boldsymbol{Z}_{\text{c}}$. For a single conductor during a fault in the reverse and forward directions, D^{f} can be calculated using (16) and (17), respectively[38]:

$$D^{\text{f}} = (1 - R_{\text{c}}/Z_{\text{c}})U_{\text{f}}, \tag{16}$$

$$D^{\text{f}} = [1 + R_{\text{c}}/Z_{\text{c}} + \Gamma(1 - R_{\text{c}}/Z_{\text{c}})]\, HU_{\text{f}}, \tag{17}$$

where Γ represents the reflection coefficient at the termination. Based on (16) and (17), at a discontinuity, the detection functions are no longer termination-independent.

3.3.2 Error due to Approximation of Transformation Matrices:

For overhead line systems with geometrically unbalanced configurations, e.g., vertical symmetric monopolar and vertical bipolar configurations, the transformation matrices will exhibit strong frequency dependency. In the time domain, using frequency dependent transformation matrices would result in convolutions, which are computationally inefficient.

To achieve computationally efficient algorithms, the real and constant transformation matrices of balanced systems are used for unbalanced systems [36]. For balanced systems, the same matrices can be used for transformation of voltage and current to the modal domain. The resulting detection function is:

$$\boldsymbol{D}_{\text{mode}}^{\text{f,b}} = \hat{\boldsymbol{T}}^{-1}\boldsymbol{U}_{\text{r}} \mp \boldsymbol{R}_{\text{c,mode}}\hat{\boldsymbol{T}}^{-1}\boldsymbol{I}_{\text{r}}, \tag{18}$$

where $\hat{\boldsymbol{T}} = \hat{\boldsymbol{T}}_{\text{u}} = \hat{\boldsymbol{T}}_{\text{i}}$. Since the convolutions are replaced by a multiplication, this results in computationally efficient algorithms in the time domain. However, the use of a constant transformation matrix will be a source of error in detection functions, since these constant matrices in general do not result in perfectly decoupled modes.

4 Wave Propagation Analysis in HVDC Grids

In this section, wave propagation characteristics are analyzed for symmetric monopolar and bipolar HVDC grid configurations with cable and overhead lines.

4.1 HVDC Grid Configurations and Transmission Lines

The transmission system layouts considered for the studies involving cables are shown in Fig. 1a and b. Submarine cables are considered with core conductor, sheath and armor. The cable parameters for the positive and negative poles are those given in [39]. The metallic return conductor is modeled with the same parameters, except that within this paper the main insulation thickness is lowered to 16 mm for demonstration purposes within this paper. The cables are buried one meter below the ground surface, and the distances between the centres of the cable core are one meter. For these cases, the sheath and armor are assumed to be perfectly grounded.

Similar to cable systems, two types of overhead line systems are considered, including two conductors for symmetric monopole and bipolar systems with ground return and three conductors for bipolar systems with metallic return. The overhead line configurations considered for the symmetrical and bipolar systems are shown in Fig. 1c and d. The maximum conductor sag along the line is 13.9 m. The line resistance is 0.0578 Ω/km and the ground resistivity is 100 Ωm.

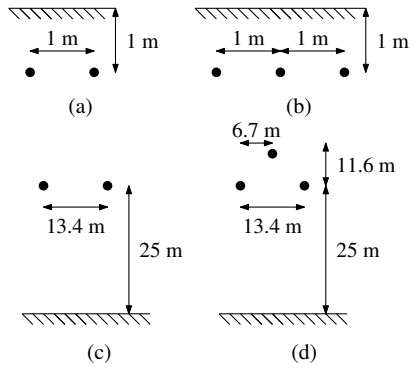

Fig. 1: Cable and overhead line configurations for (a,c) symmetrical and (b,d) bipolar systems.

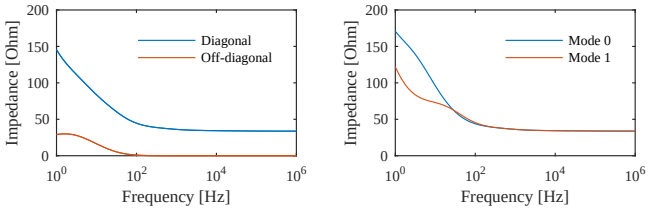

Fig. 2: (a) Phase and (b) modal characteristic impedance matrices for the symmetrical cable system.

4.2 *Cable Systems*

4.2.1 Symmetrical Monopole: A symmetrical monopole cable system with grounded sheath and armor has two propagation modes, i.e., cable and ground return. For the system of Fig. 1a, due to the balanced cable configuration, $\boldsymbol{T}_{\mathrm{u}}^{-1}$ is a matrix with real and constant values and is given by:

$$\begin{bmatrix} U_{\mathrm{mode0}} \\ U_{\mathrm{mode1}} \end{bmatrix} = \begin{bmatrix} 0.71 & 0.71 \\ 0.71 & -0.71 \end{bmatrix} \begin{bmatrix} U_{\mathrm{positive}} \\ U_{\mathrm{negative}} \end{bmatrix}, \tag{19}$$

where the first and second rows represent the ground and cable return modes, respectively.

At high frequencies, the modal domain characteristic impedances approach the diagonal elements of $\boldsymbol{Z}_{\mathrm{c,phase}}$, since the off-diagonal elements in $\boldsymbol{Z}_{\mathrm{c,phase}}$ approach zero (Fig. 2. For modes 0 and 1, $Z_{\mathrm{c,mode}}$ is equal to the sum and difference of the diagonal and off-diagonal elements of $\boldsymbol{Z}_{\mathrm{c,phase}}$, respectively [40]. In the test system of Fig. 1a, the off-diagonal elements in $\boldsymbol{Z}_{\mathrm{c,phase}}$ approach zero for frequencies above 100 Hz, Fig. 2.

4.2.2 Bipolar Cable Systems: A bipolar cable system with all sheath and armor conductors grounded has three propagation modes. For the bipolar cable system of Fig. 1b, the real part of $\boldsymbol{T}_{\mathrm{u}}^{-1}$, evaluated at 10 kHz, is:

$$\begin{bmatrix} U_{\mathrm{mode1}} \\ U_{\mathrm{mode2}} \\ U_{\mathrm{mode3}} \end{bmatrix} = \begin{bmatrix} 0.71 & 0 & 0.71 \\ 0 & 1 & 0 \\ 0.71 & 0 & -0.71 \end{bmatrix} \begin{bmatrix} U_{\mathrm{positive}} \\ U_{\mathrm{metallic}} \\ U_{\mathrm{negative}} \end{bmatrix}. \tag{20}$$

Based on (20), modes 1 and 3 are ground and cable return modes associated with the positive and negative pole and mode 2 is a ground return mode associated with the metallic return conductor. The transformation matrix elements exhibit strong frequency dependency below 1000 Hz (Fig. 3).

Similar to the symmetrical cable system, the off-diagonal elements in $\boldsymbol{Z}_{\mathrm{c,phase}}$ approach zero for frequencies above 100 Hz, whereas the diagonal elements approach the modal domain characteristic impedances (Fig. 4). The characteristic impedances of the

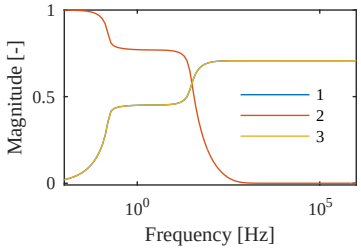

Fig. 3: Magnitude of the elements of the second row of the voltage transformation matrix for the bipolar cable system.

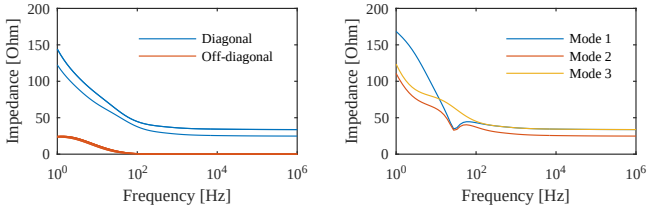

Fig. 4: (a) Phase and (b) modal characteristic impedance matrices for bipolar cable system.

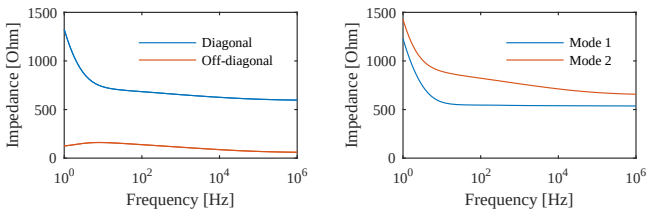

Fig. 5: (a) Phase and (b) modal characteristic impedance matrices for symmetric overhead line system.

modes associated with the pole conductors, i.e., modes 1 and 3, are equal and differ from that associated with the metallic return conductor, i.e., mode 2.

4.3 *Overhead Line Systems*

4.3.1 Symmetric Overhead Line Systems: In a symmetric overhead line system, two propagation modes exist, i.e., ground return and aerial [40]. The aerial mode propagates between the two pole conductors and exhibits lower attenuation as well as lower frequency dependency compared to the ground return mode [40].

In the symmetric overhead line system of Fig. 1c, the transformation matrix is frequency independent and is given in (19). In this system, the aerial mode (mode 1) exhibits low dependency on high frequencies, whereas the ground return mode (mode 2) depends on frequency significantly (Fig. 5b). As for the symmetrical cable system, the modal characteristic impedances are the sum and difference of the diagonal and off-diagonal elements of $\boldsymbol{Z}_{\mathrm{c,phase}}$, respectively. Unlike the cable system, $Z_{\mathrm{c,mode1}}$ and $Z_{\mathrm{c,mode2}}$ are unequal over the entire frequency range as the off-diagonal elements of $\boldsymbol{Z}_{\mathrm{c,phase}}$ are non-zero (Fig. 5a).

4.3.2 Bipolar Overhead Line Systems: In a bipolar overhead line system, similar to the bipolar cable system with grounded sheath and armor, three propagation modes exist.

In the bipolar overhead line system of Fig. 1c, the real part of $\boldsymbol{T}_{\mathrm{u}}^{-1}$ evaluated at 10 kHz in (21) shows that two of the propagation modes resemble aerial modes, i.e., modes 2 and 3 in (20), and one resembles a ground return mode, i.e., mode 1 in (20).

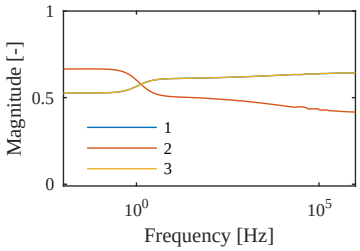

Fig. 6: Magnitude of the elements of the first row of the voltage transformation matrix for the bipolar overhead line system.

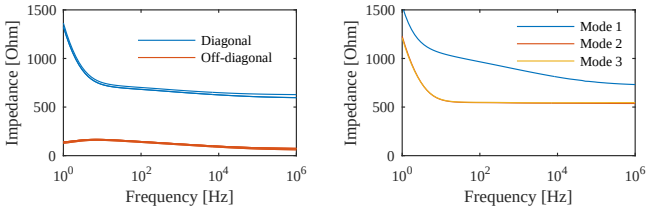

Fig. 7: (a) Phase and (b) modal characteristic impedance matrices for bipolar overhead line system.

$$\begin{bmatrix} 0.63 & 0.45 & 0.63 \\ -0.71 & 0 & 0.71 \\ -0.36 & 0.86 & -0.36 \end{bmatrix}. \tag{21}$$

As discussed in [41], the aerial modes exhibit lower attenuation and lower frequency dependency compared with the ground return mode.

Similar to the symmetrical overhead line system, the ground return mode exhibits strong frequency dependency over the entire frequency range, whereas the aerial modes exhibit low-frequency dependency above 50-100 Hz (Fig. 7).

5 Guidelines for Protection Algorithm Design

5.1 Cable Systems

Due to the low coupling between the poles in symmetric monopolar and bipolar cable systems, the modal domain neither offers considerable advantages in decoupling the wave propagation equations nor results in a simpler form of replica surge impedance. Due to the similar frequency-dependency of the characteristic impedance in both domains, the impact of using an approximate of $\boldsymbol{R}_{\mathrm{c}}$ in detection functions is the same in both domains. As concluded in [42], wave propagation on the millisecond time scale can be considered independent for each pole even in the phase domain. Therefore, for fast protection algorithms design in cable systems, the preferred domain is the phase.

Considering the off-diagonal elements of $\boldsymbol{Z}_{\mathrm{c,phase}}$ which are zero for frequencies above 100 Hz, the voltage wave at the fault location for a pole-to-ground fault at pole k can be obtained with [6]:

$$U_{\mathrm{f}}^{(k)} = -\frac{Z_{\mathrm{c}}^{(k,k)}}{(Z_{\mathrm{c}}^{(k,k)} + 2R_{\mathrm{f}})} U_{\mathrm{pre}}^{(k)}. \tag{22}$$

The detection function for all poles can be decoupled by discarding the off-diagonal elements of $\boldsymbol{R}_{\mathrm{c,phase}}$. Therefore, the proposed detection function for a cable system is:

$$\boldsymbol{D}_{\mathrm{phase}}^{\mathrm{f}} = \boldsymbol{U}_{\mathrm{phase}} - \hat{\boldsymbol{R}}_{\mathrm{c,phase}} \boldsymbol{I}_{\mathrm{phase}}, \tag{23}$$

where $\hat{\boldsymbol{R}}_{\mathrm{c,phase}} = \mathrm{diag}(\boldsymbol{R}_{\mathrm{c,phase}})$. The proposed definition of (23) results in decoupled detection functions for all poles without transformation to the modal domain, which reduces computational complexity and avoids errors introduced through the use of constant transformation matrices.

5.2 Overhead Line Systems

In overhead line systems, the modal domain offers the possibility of simplifying the replica surge impedance associated with aerial modes to a constant value. Furthermore, in geometrically balanced systems, the modal domain ideally decouples all modes in (18). In this way, the modes seen at the fault location are preserved through propagation towards the relay, although they are individually attenuated and distorted.

This section provides the necessary guidelines for fault discrimination and fault type classification in the modal domain for geometrically balanced two- and three-conductor systems.In the next section, phase and modal domain analyses in EMT-type software are provided for a study system with an unbalanced configuration.

5.2.1 Two-Conductor Systems: For symmetric systems with a flat configuration, such as the one shown in Fig. 1a, the transformation matrix is real and constant. Therefore, by using (19) or an equivalent transformation, limited error is introduced in the process of approximating $\boldsymbol{R}_{\mathrm{c,mode}}$ as the real part of $\boldsymbol{Z}_{\mathrm{c,mode}}$ for the aerial mode.

In a symmetric overhead line system, a single detection function based on the aerial mode, i.e., mode 1 in (19), is sufficient to detect all types of faults. Using (19), the transient modal voltages at the fault location approximately take the following values for positive and negative pole-to-ground and pole-to-pole faults (indicated by subscripts ptg, ntg and ptp, respectively) :

$$\begin{aligned} U_{1,\mathrm{ptg}} &= \frac{\sqrt{2}Z_{\mathrm{c},1}}{Z_{\mathrm{c},0} + Z_{\mathrm{c},1} + 4R_{\mathrm{f}}} U_{\mathrm{pre}}, \\ U_{1,\mathrm{ntg}} &= \frac{-\sqrt{2}Z_{\mathrm{c},1}}{Z_{\mathrm{c},0} + Z_{\mathrm{c},1} + 4R_{\mathrm{f}}} U_{\mathrm{pre}}, \\ U_{1,\mathrm{ptp}} &= \frac{\sqrt{2}Z_{\mathrm{c},1}}{2\,(Z_{\mathrm{c},1} + R_{\mathrm{f}})} U_{\mathrm{pre}}, \end{aligned} \tag{24}$$

where $Z_{\mathrm{c},0}$ and $Z_{\mathrm{c},1}$ are the real part of the characteristic impedances associated with ground and aerial modes evaluated at a high frequency. For the positive pole-to-ground, negative pole-to-ground and pole-to-pole faults, U_{pre} is $-U_{\mathrm{dc}}$, U_{dc} and $-2U_{\mathrm{dc}}$, respectively. For a lossless line, the detection function in the modal domain, i.e., $\boldsymbol{D}_{\mathrm{mode}}^{1}$, would take twice those values given in (24).

Compared with the expressions derived in [25], the factor multiplying the fault impedance in (24) is two times higer. The expressions derived in [25] are valid for a fault terminating the transmission line whereas (24) is valid for a fault in the middle of a transmission line.

Since the detection function takes the same sign for positive and negative pole-to-ground faults, an additional criterion is needed to discriminate between the poles. As discussed in the literature on LCC-dc systems, the polarity of the ground mode wave can be used.

5.2.2 Three-Conductor Systems: In a bipolar overhead line system, as for three-phase ac systems, various constant transformation matrices can be used to decouple the wave equations in the phase domain [43]. In a balanced three-phase system, where the two aerial modes have the same propagation constant, the condition $\boldsymbol{T}_{\mathrm{u}}^{-1} = [\boldsymbol{T}_{\mathrm{i}}]^{\mathrm{T}}$ must not strictly be satisfied [33]. In this paper, as an example, the frequency-independent transformation matrix from [36] is applied to the phase domain equations:

$$\hat{\boldsymbol{T}}^{-1} = \begin{bmatrix} 1 & 1 & 1 \\ 0 & -1 & 1 \\ 1 & 0 & -1 \end{bmatrix}. \tag{25}$$

Table 1 Modal detection functions in a three-conductor overhead line system, normalized by a $2U_{\text{pre}}$ factor as given in Section 2

	Detection Function	Ptg	Ntg	Ptn	Ptm	Ntm
D_{mode1}	$u_1 - R_{\text{c},1} i_1 = (u_n - u_m) - Z_{\text{c},1}(i_n - i_m)$	0	$\frac{3Z_{\text{c},1}}{Z_{\text{c},0}+2Z_{\text{c},1}+6R_{\text{f}}}$	$-\frac{Z_{\text{c},1}}{2Z_{\text{c},1}+2R_{\text{f}}}$	$\frac{Z_{\text{c},1}}{2Z_{\text{c},1}+2R_{\text{f}}}$	$\frac{-Z_{\text{c},1}}{Z_{\text{c},1}+R_{\text{f}}}$
D_{mode2}	$u_2 - R_{\text{c},2} i_2 = (u_p - u_n) - Z_{\text{c},1}(i_p - i_n)$	$\frac{3Z_{\text{c},1}}{Z_{\text{c},0}+2Z_{\text{c},1}+6R_{\text{f}}}$	$\frac{-3Z_{\text{c},1}}{Z_{\text{c},0}+2Z_{\text{c},1}+6R_{\text{f}}}$	$\frac{Z_{\text{c},1}}{Z_{\text{c},1}+R_{\text{f}}}$	$\frac{Z_{\text{c},1}}{2Z_{\text{c},1}+2R_{\text{f}}}$	$\frac{Z_{\text{c},1}}{2Z_{\text{c},1}+2R_{\text{f}}}$
D_{mode3}	$(u_p - u_m) - Z_{\text{c},1}(i_p - i_m)$	D_{mode2}	0	$D_{mode2}/2$	$2D_{mode2}$	$-D_{mode2}$
D_{mode4}	$(2u_n - u_m - u_p) - Z_{\text{c},1}(2i_n - i_m - i_p)$	$-D_{mode2}$	$-2D_{mode2}$	$-3/2D_{mode2}$	0	$-3D_{mode2}$
D_{mode5}	$(2u_p - u_n - u_m) - Z_{\text{c},1}(2i_p - i_n - i_m)$	$2D_{mode2}$	D_{mode2}	$3/2D_{mode2}$	$3D_{mode2}$	0
D_{mode6}	$(2u_m - u_p - u_n) - Z_{\text{c},1}(2i_m - i_p - i_n)$	$-D_{mode2}$	D_{mode2}	0	$-3D_{mode2}$	$3D_{mode2}$

In (25), rows 1-3 are associated with the ground return mode, aerial mode with currents in the metallic return and negative pole, and aerial mode with currents in positive and negative poles, respectively.

Since the aerial modes exhibit low frequency dependency and provide enough information to detect all fault types, the detection functions associated with these modes, D_{mode1} and D_{mode2} can be used in protection relays of bipolar overhead line systems. These functions are shown in Table 1, where u and i denote the transient components of measured voltages and currents. Subscripts p, n and m denote the positive pole, negative pole and metallic return conductors, respectively. Since the characteristic impedances of aerial modes exhibit low dependency on frequency, $R_{\text{c},1}$ in (18) can be replaced by $\Re\left(Z_{\text{c},1}(\omega^*)\right)$, where $Z_{\text{c},1}(\omega^*)$ is the modal characteristic impedance of aerial modes evaluated at a high frequency ω^*.

For a forward fault on a lossless line with perfect matching between $R_{\text{c},1}$ and $Z_{\text{c},1}$, detection functions based on aerial modes will detect twice the magnitude of the voltage wave U_{f}. Table 1 lists the values of detection functions D_{mode1} and D_{mode2} for most common fault types. These values are the discriminating feature associated with a certain fault type.

To detect all fault types and to determine their type, linear combinations of detection functions associated with aerial modes can be used. This concept proposed for ac systems in [44], is equally valid for dc systems. For each type of fault, one of the detection functions in Table 1 becomes zero.

As an important conclusion, the discriminating features of the fault given in Table 1, which are valid at the fault location, are preserved at the relay location through decoupled propagation along the transmission line.

6 Case Study

The test system of Fig. 8 is used to illustrate the selection of the appropriate domain for protection algorithm design. As symmetric monopolar systems are already well documented in the literature, a test system, which has a bipolar configuration with overhead lines, is selected. In this system, the pole-to-ground voltage is 320 kV and the grid is assumed to be solidly grounded at every terminal. In the analysis, the bipolar overhead line and cable configurations and parameters as discussed in Section 4.1 are used. Series inductors of 100 mH are placed at the positive and negative pole conductors, whereas no inductors are connected to the metallic return conductor. The parameters of the half-bridge modular multilevel converters (MMC) are given in Table 2.

Simulation studies are performed in PSCAD with a time step of 5 μs. The transmission lines are modeled using the frequency-dependent phase model, which is available in PSCAD. For the MMCs, the model presented in [45] is used. The faults under study are positive pole-to-ground and positive pole-to-metallic return at 25 km from MMC1, on lines L_{13} and L_{12}, respectively. The voltage and current u_r and i_r, measured at the line end of MMC2 for a period of 0.5 ms after the wave arrival at the relay location, are used in the detection functions. The lengths of L_{12}, L_{13}, L_{14} and L_{24} are 100, 200, 300 and 200 km, respectively.

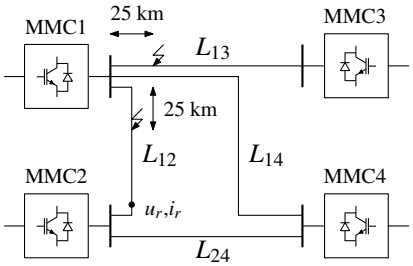

Fig. 8: Grid topology of the test system.

Table 2 Converter parameters

Parameter	Value
Rated Power	1000 MVA
Converter side ac voltage	185 kV
Grid side ac voltage	400 kV
Transformer Impedance Voltage	15%
Arm inductance	16.3 mH
Arm capacitance	65 μF
Arm resistance	0.5 Ω
Dc side inductance	10 mH

6.1 Cable System

To construct the detection functions, the following replica surge impedance matrix is used:

$$\hat{\boldsymbol{R}}_{\text{c,phase}} = \begin{bmatrix} 33.78 & 0 & 0 \\ 0 & 24.81 & 0 \\ 0 & 0 & 33.78 \end{bmatrix}, \tag{26}$$

which corresponds to the real part of the surge impedance matrix evaluated at a frequency of 1 MHz.

For cable systems, internal and external faults can be discriminated and the fault type can be determined using the phase domain. Shortly after fault inception, the propagation of waves on the cables is largely decoupled per pole. As a consequence, the detection functions in the phase domain only take high values for the faulted poles, as, e.g., illustrated for a positive pole-to-ground and positive pole-to-metallic return fault in Fig. 9.

6.2 Overhead Line System

6.2.1 Phase Domain Analysis: To avoid convolutions and considering that the off-diagonal elements are small in comparison with those on the diagonal, a real and constant diagonal matrix is chosen for $\hat{\boldsymbol{R}}_{\text{c,phase}}$. In $\hat{\boldsymbol{R}}_{\text{c,phase}}$, the diagonal elements are set equal to the characteristic impedance of the aerial mode, i.e., 543 Ω.

The fault detection in the phase domain for the test system of Fig. 8 is illustrated in Fig. 10, where the phase domain detection functions are constructed using (23). In Fig. 10, D_{phase1}, D_{phase2}, and D_{phase3} are the detection functions associated with the diagonal elements of $\boldsymbol{D}^{\text{f}}_{\text{phase}}$.

For non-unit protection algorithms, in the case study, fault discrimination can be achieved using phase domain quantities. For F_2,

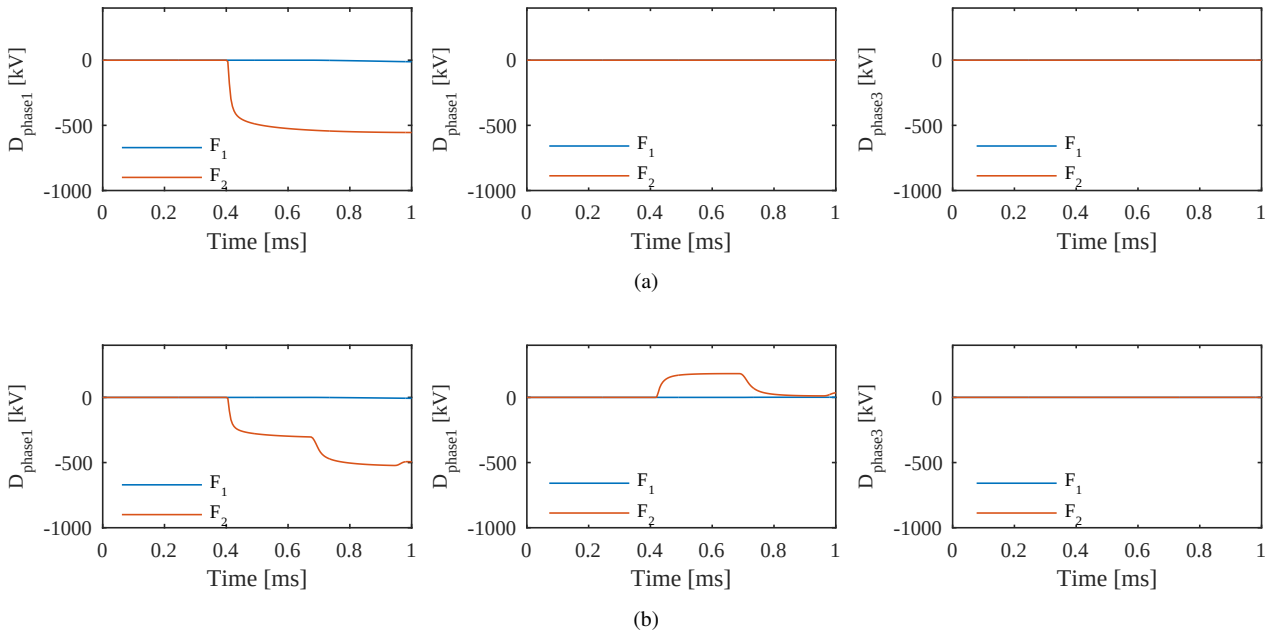

Fig. 9: Phase domain detection functions for (a) positive pole-to-ground and (b) pole-to-metallic return faults in bipolar cable system.

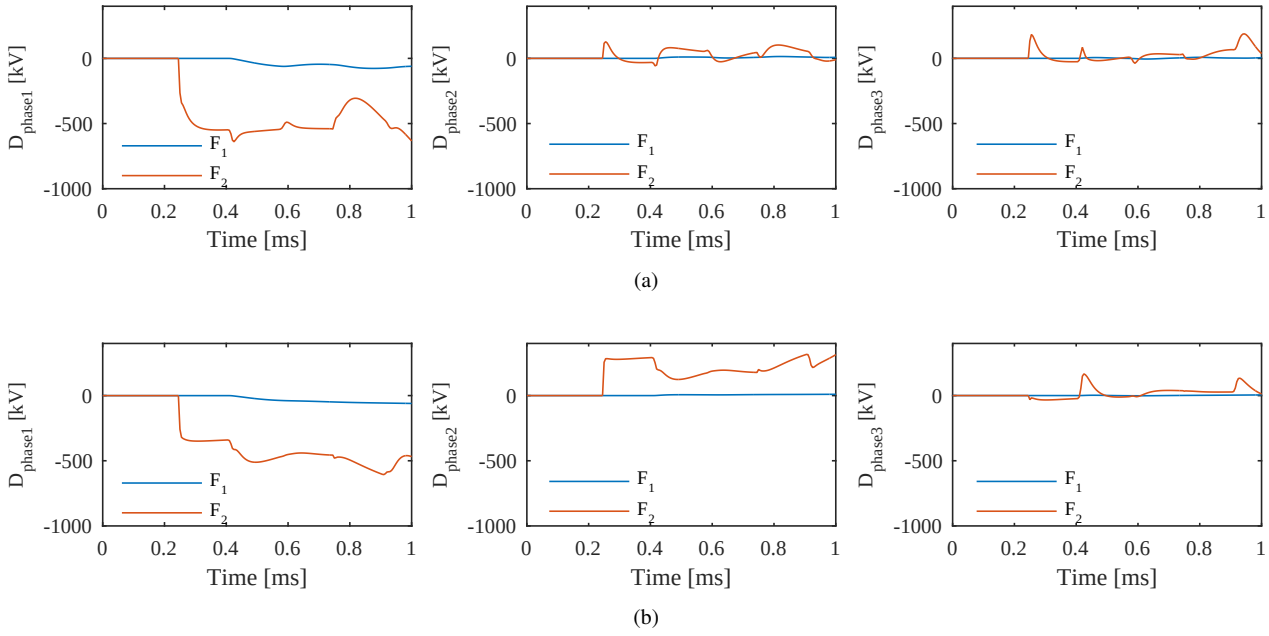

Fig. 10: Phase domain detection functions for (a) positive pole-to-ground and (b) pole-to-metallic return faults in bipolar overhead line system.

the detection function associated with the positive pole almost immediately (after the wave arrival at the relay) reaches a high value, whereas the detection function of F_1 takes a comparatively small values.

Fast fault type classification and faulted pole identification is difficult to achieve if ultra-fast operation or high sensitivity is required. For pole-to-ground faults, the first peak in the detection functions associated with metallic return and negative pole achieve a maximum absolute value of 127 and 183 kV, respectively, and fluctuate around zero during the first few milliseconds after the wave arrival (Fig. 10a). To achieve fault type classification, either a high threshold or a long time-frame is needed, possibly in conjunction with low-pass filters. In the first case, the algorithm's sensitivity is reduced whereas in the latter, the algorithm becomes slow.

6.2.2 Modal Domain Analysis: The modal domain waveforms provide a straightforward approach to fault discrimination and fault type classification, as shown in Fig. 11, where the detection functions for the internal (F_2) and external faults (F_1) show a clear distinction. However, for fault type classification and faulted pole selection, care should be taken since the modal detection functions deviate from their ideal values.

As discussed in Section 5, the mode taking a zero value can be used to determine the fault type. However, these modes may take non-zero values due to two main reasons: i) errors introduced by the non-ideal transformation matrices for the first incident wave and ii) reflections of the traveling waves at the fault location. As an example, D_{mode1} and D_{mode4} are non-zero within the time interval [0.2,0.4] in Figs. 11a and 11b, respectively. The maximum absolute values of the first peak are lower compared with phase domain

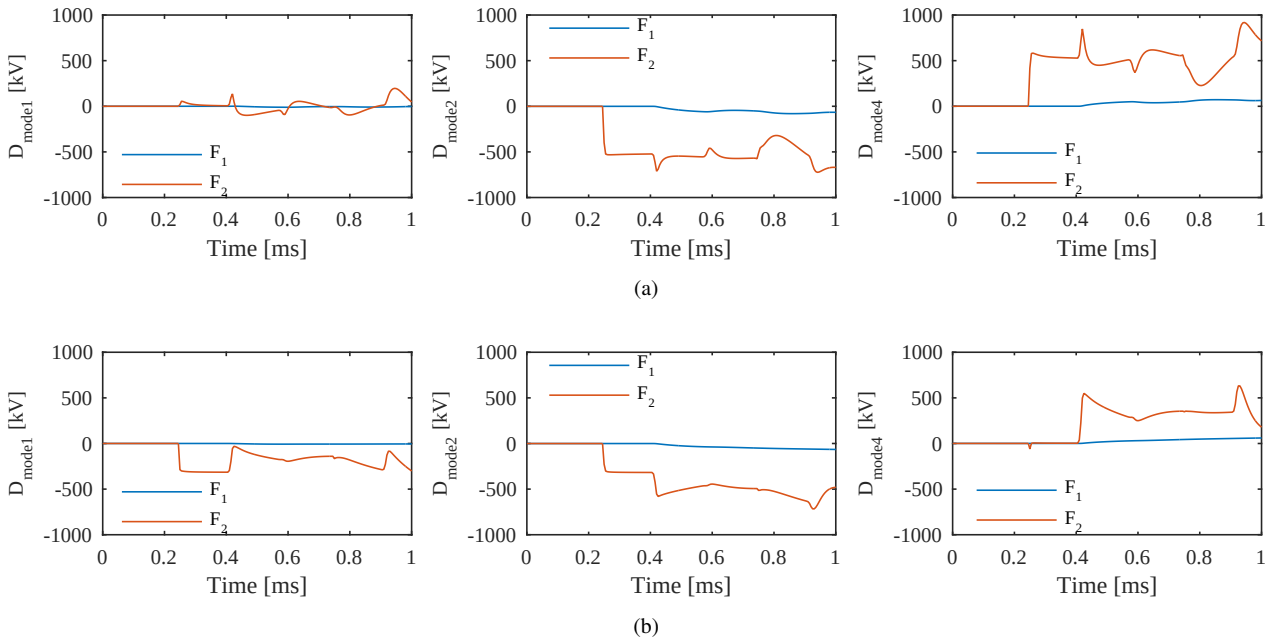

Fig. 11: Modal domain detection functions for (a) positive pole-to-ground and (b) pole-to-metallic return faults in bipolar overhead line system.

quantities, i.e., 55 and 60 for D_{mode1} and D_{mode4}. This allows for an increased sensitivity or speed of the algorithm compared with its phase domain implementation. Furthermore, for pole-to-ground and pole-to-metallic return faults at F_2, D_{mode1} and D_{mode4} exhibit non-zero values after $t \approx 0.41$ ms. This is the instant at which traveling waves reflected back from MMC1 onto L_{12} arrive at MMC2.

7 Conclusion

Based on traveling wave theory and the analysis of wave propagation characteristics of the different systems, this paper recommends to use phase and modal domains for the design of protection algorithms in cable- and overhead line-based HVDC grids, respectively. Based on this recommendation, this paper provides guidelines on constructing decoupled detection functions in the phase domain for cable systems by discarding the off-diagonal elements of the characteristic impedance matrix. For overhead line systems, guidelines on using decoupled detection functions in the modal domain are discussed. The newly constructed detection functions and guidelines complement the existing literature on dc and ac protection. These detection functions can be used for fault discrimination, fault type classification and faulted pole selection.

For cable systems, the phase domain is recommended as i) pole conductors exhibit low coupling at high frequencies and ii) even for balanced configurations, the frequency dependency of the characteristic impedance cannot be eliminated by transformation to the modal domain. For overhead lines, the modal domain is recommended since it provides a natural way for fault type classification and mitigates the strong frequency-dependency of the characteristic impedance in the phase domain. In the modal domain, each fault type has a discriminating feature which is moreover preserved when propagating towards the relay, since unlike in the phase domain, propagation of modes is decoupled. A case study using a bipolar HVDC grid shows the advantages of the phase and modal domains for cable and overhead line systems, respectively. Moreover, it shows that for overhead line systems, the errors induced by a constant transformation matrix must be taken into account.

8 References

1 D. Van Hertem, M. Ghandhari, J. Curis, O. Despouys, and A. Marzin, "Protection requirements for a multi-terminal meshed dc grid," in *CIGRÉ 2011 Bologna Symp.*, Bologna, Italy, 13-15 Sep. 2011, 8 pages.

2 F. Dijkhuizen and B. Berggren, "Zoning in high voltage dc (HVDC) grids using hybrid dc breaker," in *EPRI HVDC and FACTS Conference*, Palo Alto, CA, 28 Aug. 2013, 10 pages.

3 K. De Kerf, K. Srivastava, M. Reza, D. Bekaert, S. Cole, D. Van Hertem, and R. Belmans, "Wavelet-based protection strategy for dc faults in multi-terminal VSC HVDC systems," *IET Gener. Transm. Distrib.*, vol. 5, no. 4, pp. 496–503, Apr. 2011.

4 J. Descloux, "Protection contre les courts-circuits des réseaux à courant continu de forte puissance," Ph.D. dissertation, Université Grenoble Alpes, Grenoble, France, Sep. 2013.

5 R. E. Torres-Olguin and H. K. Hoidalen, "Inverse time overcurrent protection scheme for fault location in multi-terminal HVDC," in *Proc. IEEE Powertech*, Eindhoven, The Netherlands, 29 Jun.- 2 Jul. 2015, 6 pages.

6 W. Leterme, J. Beerten, and D. Van Hertem, "Nonunit protection of hvdc grids with inductive dc cable termination," *IEEE Trans. Power Del.*, vol. 31, no. 2, pp. 820–828, 4 2016.

7 J. Sneath and A. D. Rajapakse, "Fault Detection and Interruption in an Earthed HVDC Grid Using ROCOV and Hybrid DC Breakers," *IEEE Trans. Power Del.*, vol. 31, no. 3, pp. 973–981, Jun. 2016.

8 S. Pirooz Azad and D. Van Hertem, "A fast local bus current-based primary relaying algorithm for hvdc grids," *IEEE Trans. Power Del.*, vol. 32, no. 1, pp. 193–202, Feb 2017.

9 J. Descloux, B. Raison, and J.-B. Curis, "Protection algorithm based on differential voltage measurement for MTDC grids," in *Proc. IET DPSP 2014*, 31 Mar.-3 Apr. 2014, 5 pages.

10 A. Adamczyk, C. D. Barker, and H. Ha, "Fault detection and branch identification for HVDC grids," in *Proc. IET DPSP 2014*, Mar. 31 Mar.- 3 Apr. 2014, 6 pages.

11 M. Hajian, L. Zhang, and D. Jovcic, "DC Transmission Grid With Low-Speed Protection Using Mechanical DC Circuit Breakers," *IEEE Trans. Power Del.*, vol. 30, no. 3, pp. 1383–1391, 6 2015.

12 D. Tzelepis, A. Dysko, G. Fusiek, J. Nelson, P. Niewczas, D. Vozikis, P. Orr, N. Gordon, and C. Booth, "Single-ended differential protection in mtdc networks using optical sensors," *IEEE Trans. Power Del.*, vol. PP, no. 99, pp. 1–1, 2016.

13 N. Johannesson and S. Norrga, "Longitudinal differential protection based on the universal line model," in *IEEE Proc. IECON 2015*, Yokohama, Japan, 9-12 Nov. 2015, pp. 1091–1096.

14 Q. Feng, G. B. Zou, C. H. Xu, H. L. Gao, and Y. Y. Ma, "A protection scheme based on polarity comparison for VSC-MTDC grids," in *Proc. IET ACDC 2016*, Bejing, China, 28-29 May 2016, 6 pages.

15 K. Padiyar, *HVDC Power Transmission Systems, Technology and System Interactions*. Delhi, India: New Age International Publishers, 1990.

16 J. Arrillaga, *High Voltage Direct Current Transmission*. Stevenage, UK: The IET, 1998.

17 H. Kunlun, C. Zexiang, and L. Yang, "Study on protective performance of HVDC transmission line protection with different types of line fault," in *Proc. IEEE DRPT*, Weihai, China, Jul. 6-9 Jul. 2011, pp. 358–361.

18 Z. Shuo and L. Yongli, "Simulation and analysis of HVDC line protection under the single pole to ground fault with high transition resistance," in *Proc. IEEE DRPT*, Weihai, China, Jul. 6-9 Jul. 2011, pp. 926–929.

19 F. Kong, Z. Hao, and B. Zhang, "A Novel Traveling-Wave-Based Main Protection Scheme for ± 800 kV UHVDC Bipolar Transmission Lines," *IEEE Trans. Power Del.*, vol. 31, no. 5, pp. 2159–2168, 10 2016.

20 J. Liu, N. Tai, C. Fan, and Y. Yang, "Transient measured impedance-based protection scheme for DC line faults in ultra high-voltage direct-current system," *IET Gener. Transm. Distrib.*, vol. 10, no. 14, pp. 3597–3609, 10 2016.

21 P. Anderson, *Power System Protection*. Hoboken, NJ, USA: J. Wiley & Sons, 1998.

22 G. Mazur, R. Carryer, S. T. Ranade, and T. WeB, "Converter control and protection of the nelson river hvdc bipole 2 commissioning and first year of commercial operation," *IEEE Trans. Power App. Syst.*, vol. PAS-100, no. 1, pp. 327–335, Jan 1981.

23 X. Liu, A. H. Osman, and O. P. Malik, "Hybrid traveling wave/boundary protection for bipolar HCDC line," in *Proc. IEEE PES GM*, Calgary, Alberta, Jul. 26-30 Jul. 2009, 8 pages.

24 Y. Zhang, N. Tai, and B. Xu, "A travelling wave protection scheme for bipolar HVDC line," in *Proc. IEEE APAP*, vol. 3, Bejing, China, Oct. 16-20 Oct. 2011, pp. 1728–1731.

25 ——, "Fault Analysis and Traveling-Wave Protection Scheme for Bipolar HVDC Lines," *IEEE Trans. Power Del.*, vol. 27, no. 3, pp. 1583–1591, Jul. 2012.

26 X. Chu, G. Song, and J. Liang, "Analytical method of fault characteristic and non-unit protection for HVDC transmission lines," *CSEE Journal of Power and Energy Systems*, vol. 2, no. 4, pp. 37–43, Dec. 2016.

27 Y. Ma, H. Li, J. Hu, J. Wu, and G. Wang, "Analysis of travelling wave protection criterion performance for double-circuit HVDC," in *Proc. IEEE APPEEC*, Knowloon, Hong Kong, Dec. 8-11 Dec. 2013, 5 pages.

28 H. Ha, Y. Yu, R. Yi, Z. Q. Bo, and B. Chen, "Novel scheme of travelling wave based differential protection for bipolar HVDC transmission lines," in *Proc. IEEE POWERCON*, Hangzhou, China, Oct. 24-28 Oct. 2010, 6 pages.

29 D. Naidoo and N. Ijumba, "HVDC line protection for the proposed future HVDC systems," in *IEEE PowerCon 2004*, vol. 2, 21-24 Nov. 2004, pp. 1327–1332.

30 I. Jahn, N. Johannesson, and S. Norrga, "Survey of methods for selective DC fault detection in MTDC grids," in *Proc. IET ACDC 2017*, Manchester, UK, Feb. 14-16 Feb. 2017, 7 pages.

31 N. Johannesson, S. Norrga, and C. Wikström, "Selective wave-front based protection algorithm for mtdc systems," in *Proc. IET DPSP 2016*, Edinburgh, UK, 7-10 Mar. 2016.

32 C. Paul, *Analysis of Multiconductor Transmission Lines*. Hoboken, NJ: John Wiley & Sons, 2008.

33 L. Wedepohl, "Application of matrix methods to the solution of travelling-wave phenomena in polyphase systems," *Electrical Engineers, Proceedings of the Institution of*, vol. 110, no. 12, pp. 2200–2212, December 1963.

34 J. Martinez-Velasco, *Power System Transients: Parameter Determination*. Boca Raton, FL: CRC Press, 2009.

35 N. Johannesson, "Method for sensing a fault in a power system based on travelling wave currents," Patent US20 150 233 976 A1, 2015.

36 M. Bollen, "On travelling-wave-based protection of high voltage networks," Ph.D. dissertation, TU Eindhoven, Eindhoven, The Netherlands, 1989.

37 A. Johns, "New ultra-high-speed directional comparison technique for the protection of e.h.v. transmission lines," *IEE Proc. C Gener., Transm. and Distr.*, vol. 127, no. 4, pp. 228–239, Jul. 1980.

38 W. Leterme, "Communication-less protection algorithms for meshed vsc hvdc cable grids," Ph.D. dissertation, KU Leuven, Leuven, Belgium, 2016.

39 W. Leterme, N. Ahmed, L. Ängquist, J. Beerten, D. Van Hertem, and S. Norrga, "A new HVDC grid test system for HVDC grid dynamics and protection studies in EMTP," in *Proc. IET ACDC*, Birmingham, UK, 10-12 Feb. 2015, 7 pages.

40 E. W. Kimbark, "Transient overvoltages caused by monopolar ground fault on bipolar dc line: theory and simulation," *IEEE Trans. Power App. Syst.*, vol. PAS-89, no. 4, pp. 584–592, Apr. 1970.

41 J. Marti, L. Marti, and H. Dommel, "Transmission line models for steady-state and transients analysis," in *Proc. IEEE APT '93*, Athens, Greece, 5-8 Sep. 1993, pp. 744–750.

42 A. Ametani, "Wave propagation characteristics of cables," *IEEE Trans. Power App. Syst.*, vol. PAS-99, no. 2, pp. 499–505, March 1980.

43 M. Mansour and G. Swift, "A multi-microprocessor based travelling wave relay - theory and realization," *IEEE Trans. Power Del.*, vol. 1, no. 1, pp. 272–279, Jan. 1986.

44 M. Bollen and G. Jacobs, "Extensive testing of an algorithm for travelling-wave-based directional detection and phase-selection by using TWONFIL and EMTP," TU Eindhoven, EUT report. E, Fac. of Electrical Engineering; Vol. 88-E-206, 1988.

45 N. Ahmed, L. Ängquist, S. Norrga, and H.-P. Nee, "Validation of the continuous model of the modular multilevel converter with blocking/deblocking capability," in *Proc. IET ACDC 2012*, Birmingham, UK, 4-6 Dec. 2012, 6 pages.